RSC Advances

PAPER

View Article Online
View Journal | View Issue

Cite this: *RSC Adv.*, 2017, **7**, 2480

Template-free synthesis of hierarchical hollow V_2O_5 microspheres with highly stable lithium storage capacity†

Hangkong Li,[a] Jiexi Wang,[ab] Xiang Liu,[c] Qian Sun,[c] Aleksandra B. Djurišić,[c] Maohai Xie,[c] Ying Mei,[a] Chuyang Y. Tang[a] and Kaimin Shih*[a]

Received 29th October 2016
Accepted 16th December 2016

DOI: 10.1039/c6ra25997a

www.rsc.org/advances

Hollow V_2O_5 microspheres were successfully synthesized by a solvothermal method and subsequent calcination. The rigid hollow V_2O_5 cathode prepared in isopropanol solvent exhibited excellent cycling performance and rate capability. Within a voltage window of 2.5 to 4 V, a maximum specific discharge capacity of 128 mA h g^{-1} was delivered at 1 A g^{-1}. Even after 500 cycles, the capacity retention was 92.2%.

The development of clean energy storage systems has become more and more important because of worsening environmental and energy issues. As one of the most successful technologies for energy storage and conversion, rechargeable lithium ion batteries (LIBs) are being widely used in portable electronic devices, electric vehicles, and hybrid electric vehicles.[1] However, to meet the urgent demand for energy devices in modern society, research into LIBs with higher energy and power density still remains a great challenge. Generally, the performance of LIBs is determined mainly by the electrode materials, especially the cathode materials, due to the relatively high capacity and stability of the anodes.[2,3] The commercial cathode materials $LiCoO_2$, $LiMn_2O_4$, and $LiFePO_4$ can only insert or deinsert one lithium ion or less per unit formula, which limits the available capacity.[4] Therefore, the development of new cathode materials for the next generation of LIBs is of great significance.

In recent decades, vanadium-based oxides such as V_2O_5,[5–7] $Li_3V_2(PO_4)_3$,[8] $LiVPO_4F$,[9] and LiV_3O_8 (ref. 10) have attracted tremendous attention as cathodes due to their high capacities, various oxidation states, abundant resources, and low cost.[11–13] Among them, layered vanadium pentoxide (V_2O_5) possesses a high theoretical capacity of 294 mA h g^{-1} (with respect to the intercalation of two lithium ions per V_2O_5 unit in 2 to 4 V).[14] Fig. S1† shows the crystal structure projection of V_2O_5 along the [010] direction, it consists of edge- or corner-sharing VO_5 square pyramids in the sequence up–up–down–down. Hence, lithium ions can freely insert into the interlayer space of this unique open structure of V_2O_5.[15] To overcome the challenges of structural deterioration during cycling, poor electric conductivity, and slow lithium ion diffusion,[16] researchers have processed V_2O_5 into different nanostructures, such as nanorods,[17] nanowires,[18] nanosheets,[19] and hierarchical microspheres.[20,21] V_2O_5 in the form of hollow structure is of particular interest. This structure offers a larger surface area, a shorter lithium ion diffusion distance, and a void space for buffering of the volume change,[22–24] resulting in improved cycling stability and rate capability.[23–29] However, the synthesis of hollow V_2O_5 often involves expensive organic vanadium sources,[23–25] as well as surfactants such as polyvinylpyrrolidone to control the hierarchical hollow structure.[25,26] Although templating method is considered as an effective strategy to fabricate the hollow V_2O_5,[27] the process is often complicated and time consuming. Pan and co-workers presented an alternative by using oxalic acid as a reductant to obtain the VOC_2O_4 precursor, and the resulting V_2O_5 hollow microspheres showed superior electrochemical performance.[28,29] To control the morphology and sizes of nanomaterials, citric acid is considered to be a good additive in the synthesis system because of its contributions to reduction and complexing during chemical reaction.[30] Therefore, we applied citric acid, acting as both a reductant and a chelating agent, to prepare hierarchical V_2O_5 hollow structures.

Herein, we report the template-free synthesis of the hollow V_2O_5 microspheres *via* a solvothermal method combined with heat treatment. A detailed experimental section can be found in the ESI.† The formation mechanism of the hollow structures has been investigated. After calcination, the hollow microspheres were well preserved. As cathodes for LIBs, the nanoparticle-assembled V_2O_5 microspheres obtained from isopropanol (IPA) manifested more stable cycling performance than nanosheet-assembled microspheres prepared from ethylene glycol (EG).

[a]*Department of Civil Engineering, The University of Hong Kong, Pokfulam Road, Hong Kong, China. E-mail: kshih@hku.hk*

[b]*School of Metallurgy and Environment, Central South University, Changsha, Hunan 410083, China*

[c]*Department of Physics, The University of Hong Kong, Pokfulam Road, Hong Kong, China*

† Electronic supplementary information (ESI) available: Experimental details; crystal structure of V_2O_5; XRD data of the precursors and the final products; SEM and TEM patterns of the precursors; CV curves of V_2O_5–EG electrode; *ex situ* SEM images of the V_2O_5–IPA and V_2O_5–EG electrodes; cycling performance of the V_2O_5–IPA and V_2O_5–EG electrodes at 3 A g^{-1}. See DOI: 10.1039/c6ra25997a

Furthermore, the morphological changes of these two electrodes under different lithiation/delithiation levels or after cycling are discussed in details. To our best knowledge, this electron microscopic investigation on the changes of the hollow V_2O_5 microspheres were not reported before.

The vanadyl citrate ($VOC_6H_6O_7$) solution was firstly prepared with V_2O_5 and citric acid.[31] The hollow precursors were then synthesized from the vanadyl citrate solution in IPA or EG *via* a solvothermal reaction. X-ray diffraction (XRD) was applied for phase identification of the precursors (Fig. S2a, see ESI†). However, it is difficult to index the precursors from the broad diffraction peaks due to their low crystallinity. As shown in the scanning electron microscope (SEM) and transmission electron microscope (TEM) images (Fig. 1a, b, e and f), both precursors had a hollow structure. In the IPA case, the hollow spheres consisted of nanoparticles (Fig. 1a). However, from the SEM image (Fig. 1e) of the microspheres synthesized using EG as the solvent, it can be seen that this hierarchical hollow structure was loosely assembled from nanosheets. These two forms differ from the reported IPA and EG cases using other vanadium sources,[24–29,32] which may be attributed to the effects of citrate.

After calcination in air at 350 °C, the precursors were successfully transformed into high-crystalline V_2O_5, which can be confirmed from the XRD data (Fig. S2b†). The patterns were clearly identified as orthorhombic V_2O_5 (space group: *Pmmn*, JCPDS no. 41-1426). Furthermore, the TEM images (Fig. 1d and h) of the V_2O_5 microspheres with diameters between 1 and 2 μm reveal that the hollow structure was preserved without obvious shrinkage or structural deformation. Nevertheless, the outer surfaces of these two types of microspheres changed slightly after the heat treatment. The rigid V_2O_5 microspheres obtained from IPA (designated as V_2O_5–IPA) had smoother surfaces than the precursor because of the recrystallization process during calcination (Fig. 1c). In contrast, Fig. 1g shows that the surfaces of the interconnected V_2O_5 microspheres from EG (designated as V_2O_5–EG) became rougher. This phenomenon can be explained due to the difference of the atomic diffusivity on the terminating facets between the nanoparticle and nanosheet subunits.[33] Therefore, after annealing the smooth surfaces were obtained in the V_2O_5–IPA microspheres while the V_2O_5–EG microspheres showed rough surfaces. The high resolution TEM images were provided in Fig. S3† to study the crystalline features of these two hierarchical microspheres. The lattice spacing parameters of 0.217 nm (V_2O_5–IPA) and 0.565 nm (V_2O_5–EG) matched well to the {002} and {200} planes of the orthorhombic V_2O_5, respectively.

Fig. 2 is a detailed schematic of the formation process of V_2O_5 hollow microspheres, which is similar to some reported cases for synthesis of the hollow structure.[24,28] The TEM images of the products obtained at 200 °C for different reaction times are shown in Fig. S4 and S5.† First, solid microspheres were formed as a result of the reaction between vanadyl citrate and the organic solvents (6 h, Fig. S4a and S5a†). With increasing reaction time, the interior substance with high surface energy began to dissolve and move to the outer surface for recrystallization, which is known as the inside–out Ostwald-ripening process (12 to 20 h, Fig. S4b and c and S5b and c†). When the reaction time was further prolonged, a completely hollow structure could be achieved (24 h, Fig. S4d and S5d†). Finally, after calcination, hierarchical hollow V_2O_5 microspheres were obtained. Moreover, the morphological changes were studied by adjusting the vanadyl citrate concentrations. As shown in Fig. S6,† when the $VOC_6H_6O_7$ concentration decreased, the average size of the microspheres obtained from IPA decreased and the inhomogeneity of the material appeared. Similarly, in the EG case (Fig. S7†), the density of microspheres was less as the $VOC_6H_6O_7$ concentration decreased. In addition, other vanadium sources such as VOC_2O_4 (ref. 28) and V_2O_5 sol[5] solutions were also used for comparison. Under our experimental conditions, the shape and size of the microspheres in

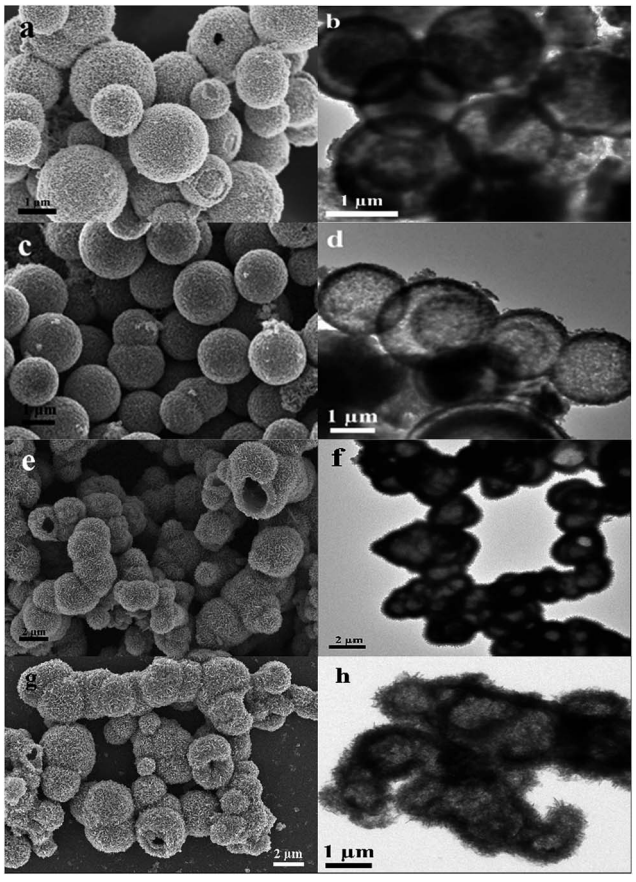

Fig. 1 SEM and TEM images of precursors ((a and b) for IPA case; (e and f) for EG case) and final products after calcination ((c and d) are from V_2O_5–IPA; (g and h) are from V_2O_5–EG).

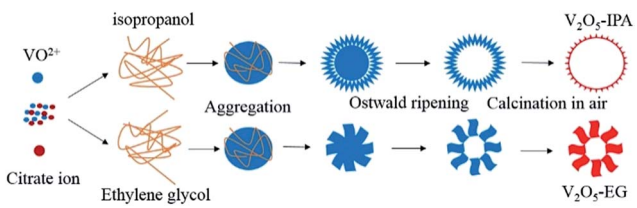

Fig. 2 Schematic illustration of synthesis of hollow V_2O_5–IPA and V_2O_5–EG microspheres.

this work were different from those prepared from VOC_2O_4 (Fig. S8a and b†). When using V_2O_5 sol, only nanobelts and nanosheet-networks were formed (Fig. S8c and d†), and this shows the important role of vanadyl citrate in the synthesis of hollow microspheres.

As revealed by the nitrogen adsorption–desorption measurement, the Brunauer–Emmett–Teller (BET) specific surface areas for V_2O_5–IPA and V_2O_5–EG were 33 and 58 $m^2\ g^{-1}$, respectively. The sorption isotherms (Fig. 3a and c) of these two hollow structures are consistent with type IV curves, including H3 hysteresis loops.[34] In Fig. 3b and d, the pore size distribution plots indicate the presence of mesopores with diameters of about 2 and 40 nm. Overall, the nanosheet-assembled V_2O_5–EG hollow microspheres with interconnected morphology exhibited larger specific surface areas than the smooth and rigid V_2O_5–IPA hollow microspheres.

Cyclic voltammetry (CV) curves of V_2O_5–IPA in the voltage range of 2.5 to 4 V were first measured to investigate the Li ion insertion and deinsertion behavior. As shown in Fig. 4, two strong cathodic peaks at around 3.36 and 3.15 V *vs.* Li/Li^+ were clearly observed, which indicates the two-step intercalation of one Li ion into the V_2O_5 matrix and the phase transitions from α-V_2O_5 to ε-$Li_{0.5}V_2O_5$ and then to δ-LiV_2O_5.[35] The corresponding potential peaks at 3.27 and 3.45 V *vs.* Li/Li^+ during the anodic scanning suggest the reversible Li ion extraction process from δ-LiV_2O_5 to ε-$Li_{0.5}V_2O_5$ and then to α-V_2O_5. In addition, the first three CV curves with well-defined peaks almost overlapped, implying the highly reversibility of the V_2O_5–IPA electrodes. The similar CV curves of V_2O_5–EG are also shown in Fig. S9.†

Galvanostatic charging/discharging measurement was performed to investigate the long-term cyclic stability of the V_2O_5–IPA and V_2O_5–EG electrodes in the voltage range of 2.5 to 4 V. As shown in Fig. 5a, there is no great difference between these two cycling profiles. The maximum discharge capacities reached 135 and 140 mA h g^{-1} (close to the theoretical value of 147 mA h g^{-1} when one lithium ion is inserted in 2.5 to 4 V) at a current

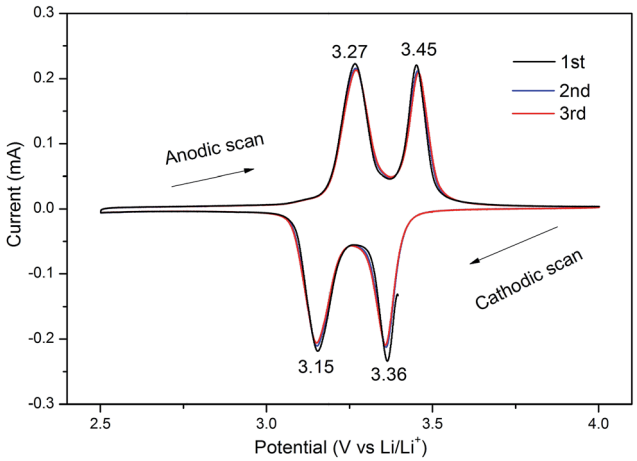

Fig. 4 Three successive CV curves of the V_2O_5–IPA electrode.

density of 300 mA g^{-1} for the V_2O_5–IPA and V_2O_5–EG electrodes, respectively. Interestingly, there was an increasing trend of the discharge capacity during the first several cycles, which has also been found in some vanadium-based compounds.[36] The increased capacity may also be attributed to the activation, stabilization and fully wetting of the electrodes in the initial cycles.[35,36] After 300 cycles, a capacity of 123 mA h g^{-1} was retained for the V_2O_5–IPA electrode, with an average capacity fading rate of 0.03% per cycle. The V_2O_5–EG electrode exhibited higher discharge capacities than V_2O_5–IPA in the beginning. However, its capacity decreased to 122 mA h g^{-1} after 300 cycles, with a relatively high fading rate of 0.043% per cycle. The large specific surface area is believed to shorten the Li ion diffusion distance and enlarge the electrode/electrolyte contact interface, thereby enhancing the Li storage capability. As a result, the V_2O_5–EG hollow microspheres, with a larger surface area, showed better electrochemical performance than V_2O_5–IPA, especially at the beginning of the cycles. Nevertheless, the capacity advantage of V_2O_5–EG only lasted for the first dozen cycles. This difference became more obvious when the current density was increased.

The cycling performance of the V_2O_5–IPA and V_2O_5–EG electrodes at a high current density of 1 A g^{-1} is shown in Fig. 5b. The maximum specific discharge capacities were 128 and 136 mA h g^{-1} for V_2O_5–IPA and V_2O_5–EG cathodes, respectively. Remarkably, the capacity of the V_2O_5–IPA electrode was retained at 118 mA h g^{-1} after 500 cycles, which corresponded to 92.2% of the maximum capacity. The result is comparable to many published V_2O_5 electrodes (Table S1†). However, even though the V_2O_5–EG electrode exhibited higher capacity in the first 50 cycles than the V_2O_5–IPA electrode, only 79% of its maximum capacity was preserved after 300 cycles. The rapid capacity fading rate (0.07% per cycle) of the V_2O_5–EG electrode may be attributed to the structural collapse of the loose hollow microspheres during cycling. In contrast, the rigid V_2O_5–IPA hollow microspheres with excellent cycling performance can buffer the volume change effectively and hence are more stable during the Li insertion/deinsertion process. This was confirmed by the SEM images of these two electrodes under

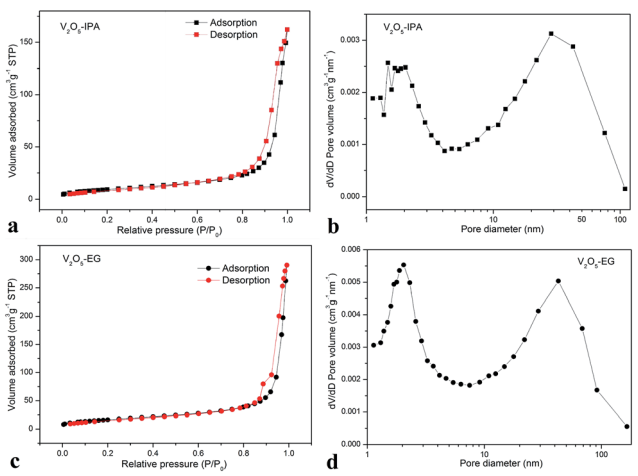

Fig. 3 Nitrogen adsorption–desorption isotherms of V_2O_5–IPA (a) and V_2O_5–EG (c) and their corresponding pore-size-distribution curves (b and d).

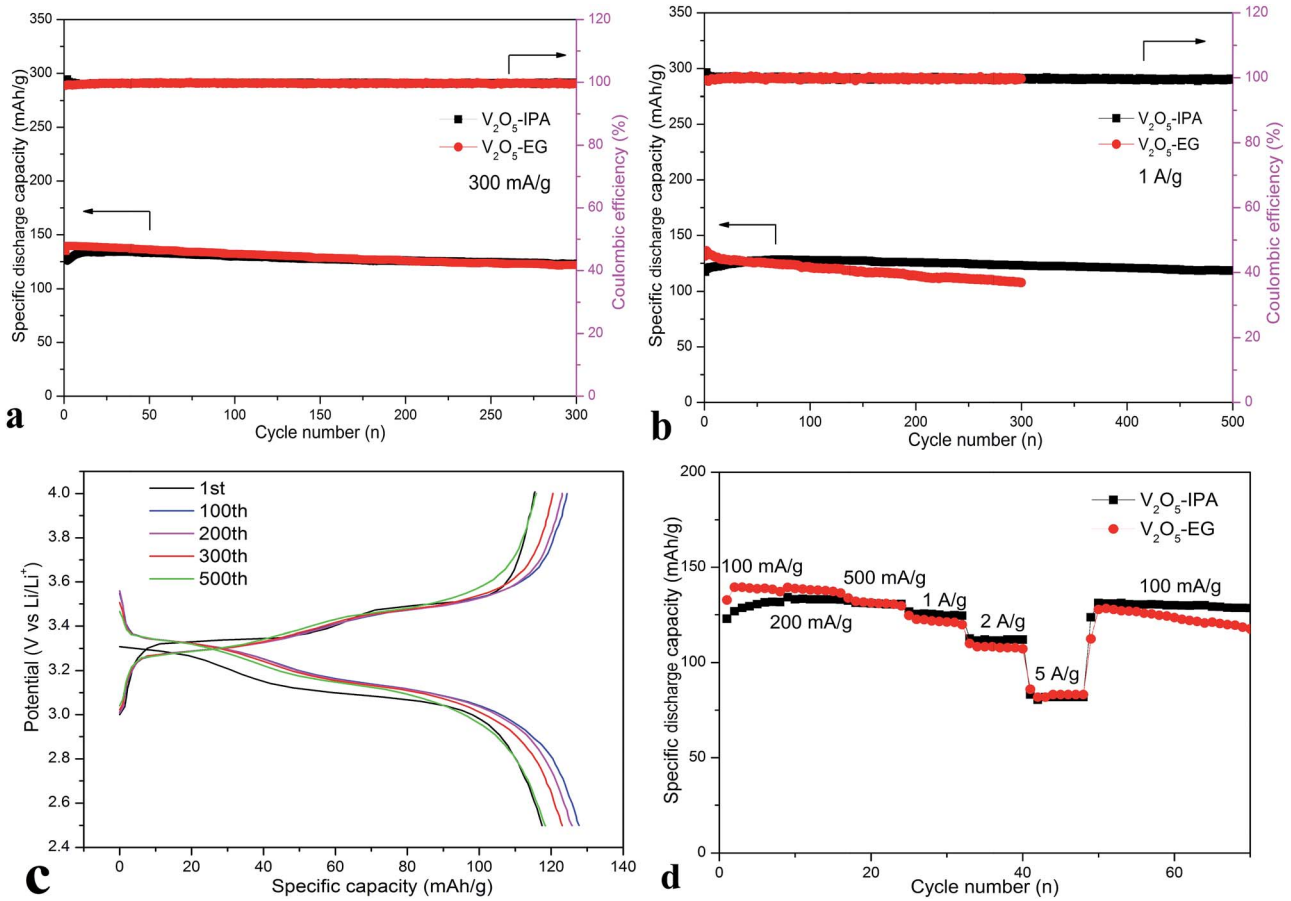

Fig. 5 Electrochemical performances of V_2O_5–IPA and V_2O_5–EG electrodes. (a) and (b) show cycling performance of these two electrodes at current density of 300 mA g^{-1} and 1A g^{-1}, respectively; (c) the charge–discharge profiles of V_2O_5–IPA electrode for different cycle numbers at 1A g^{-1}; (d) rate performance of V_2O_5–IPA electrode.

different charge/discharge states or after cycling. In Fig. S10,† It can be seen that there was little difference between these microspheres under various states. Even after 300 cycles, the intact V_2O_5–IPA microspheres could be clearly observed, which indicates the volume expansion during cycling had less effect on the rigid hollow structure. However, as shown in Fig. S11,† micro-spherical features of V_2O_5–EG material gradually disappeared and the volume changes increased with the more intensive charge/discharge operation. Moreover, even after dispersal in ethanol for 1 month, the V_2O_5–IPA microspheres were more stable than the completely collapsed V_2O_5–EG hollow microspheres (Fig. S12†). The above results reveal the good structural stability of the V_2O_5–IPA electrode. For both electrodes, the coulombic efficiency remained close to 100% throughout the cycling test, suggesting their excellent reversibility. Moreover, Fig. 5c displays the discharge–charge curves of the V_2O_5–IPA electrode for the 1st, 100th, 200th, 300th, and 500th cycles at 1 A g^{-1}. All of the profiles show similar two-step voltage plateaus related to the typical lithiation and de-lithiation process of V_2O_5, which are consistent with the CV curves. Fig. S13† shows the cycling behavior of these two electrodes at a current density of 3 A g^{-1}. The maximum discharge capacities even reached 115 and 132 mA h g^{-1} for the V_2O_5–IPA and V_2O_5–EG electrodes, with capacity retention of 80% and 57% after 300 cycles, respectively. Unsurprisingly, the V_2O_5–IPA electrode exhibited more stable cycling performance than the V_2O_5–EG electrode.

The rate performance of these two electrodes at different current densities was also investigated. Fig. 5d demonstrates the superior rate capability of the V_2O_5–IPA cathode, with an average capacity of 129, 133, and 131 mA h g^{-1} at 100, 200, and 500 mA g^{-1}, respectively. At 1 A g^{-1}, the average capacity reached 125 mA h g^{-1}, corresponding to 94% of the maximum capacity (133 mA h g^{-1}) during the whole rate test. The capacity retention was 84.2% (112 mA h g^{-1}) and 61.7% (82 mA h g^{-1}) at 2 A g^{-1} and 5 A g^{-1}, respectively, on the basis of the maximum capacity. When the current density was reset to 100 mA g^{-1}, a specific capacity of 131 mA h g^{-1} could be recovered. For the rate performance of the V_2O_5–EG electrode, a high specific capacity of 140 mA h g^{-1} was delivered at 100 mA g^{-1}. The V_2O_5–EG electrode displayed a higher capacity than the V_2O_5–IPA electrode at low current densities. However, the capacity began to decrease at high current density. Even after the current density was back to 100 mA g^{-1}, the fading problem became worse. This situation was similar to the cycling performance of these two electrodes. Furthermore, in terms of capacity

retention on the basis of 140 mA h g^{-1}, the values were only 87.1% (122 mA h g^{-1}), 77.1% (108 mA h g^{-1}), and 59.3% (83 mA h g^{-1}) at 1, 2, and 5 A g^{-1}, respectively. On the whole, the rigid hollow V_2O_5–IPA microspheres showed better rate capability and stability as a cathode for LIBs. The excellent electrochemical performance of the V_2O_5–IPA cathode may be attributable to the stable rigid hollow structure, which can buffer the volume change during cycling; enhanced contact area of electrode/electrolyte; and reduced lithium ion diffusion and electron transportation distance.

In summary, two types of hierarchical hollow V_2O_5 microspheres were synthesized successfully *via* a solvothermal method followed by heat treatment. The nanosheet-assembled V_2O_5 microspheres obtained from ethylene glycol solvent exhibited a high capacity of 140 mA h g^{-1} at 300 mA g^{-1} and retained 122 mA h g^{-1} after 300 cycles, which corresponds to a fading rate of 0.043% per cycle. The fading of the V_2O_5–EG electrode was severe, especially at high current densities. At first, due to the larger surface area, V_2O_5–EG showed higher discharge capacities than the V_2O_5–IPA electrode prepared from isopropanol solvent. However, as the cycles went on, the hollow microspheres of V_2O_5–EG collapsed, and the capacity quickly decreased. The V_2O_5–IPA electrode exhibited a maximum discharge capacity of 128 mA h g^{-1} at 1 A g^{-1}, with a capacity retention of 92.2% even after 500 cycles. At 3 A g^{-1}, 80% of the maximum capacity (115 mA h g^{-1}) was retained after 300 cycles. Overall, because of their outstanding structural characteristics, the rigid V_2O_5–IPA hollow microspheres can deliver excellent cycling performance and rate capability as a cathode for LIBs.

Acknowledgements

We gratefully acknowledge the funding for this research provided by the General Research Fund Scheme of the Research Grants Council of Hong Kong (17206714, 17212015) and HKU Strategic Research Themes on Clean Energy and Earth as a Habitable Planet.

Notes and references

1 (*a*) L. Mai, X. Tian, X. Xu, L. Chang and L. Xu, *Chem. Rev.*, 2014, **114**, 11828–11862; (*b*) J. X. Zhang, Z. S. Ma, J. J. Cheng, Y. Wang, C. Wu, Y. Pan and C. Lu, *J. Electroanal. Chem.*, 2015, **738**, 184–187.

2 (*a*) J. Xu, S. Dou, H. Liu and L. Dai, *Nano Energy*, 2013, **2**, 439–442; (*b*) M. Hu, X. Pang and Z. Zhou, *J. Power Sources*, 2013, **237**, 229–242; (*c*) Z. Ma, T. Li, Y. L. Huang, J. Liu, Y. Zhou and D. Xue, *RSC Adv.*, 2013, **3**, 7398–7402; (*d*) Z. Xie, Z. Ma, Y. Wang, Y. Zhou and C. Lu, *RSC Adv.*, 2016, **6**, 22383–22388.

3 (*a*) A. Devaraj, M. Gu, R. Colby, P. Yan, C. M. Wang, J. M. Zheng, J. Xiao, A. Genc, J. G. Zhang, I. Belharouak, D. Wang, K. Amine and S. Thevuthasan, *Nat. Commun.*, 2015, **6**, 8014; (*b*) J. Wang, Q. Zhang, X. Li, B. Zhang, L. Mai and K. Zhang, *Nano Energy*, 2015, **12**, 437–446; (*c*) Q. Zhang, J. Wang, J. Dong, F. Ding, X. Li, B. Zhang, S. Yang and K. Zhang, *Nano Energy*, 2015, **13**, 77–91.

4 L. Croguennec and M. R. Palacin, *J. Am. Chem. Soc.*, 2015, **137**, 3140–3156.

5 Y. Liu, M. Clark, Q. Zhang, D. Yu, D. Liu, J. Liu and G. Cao, *Adv. Energy Mater.*, 2011, **1**, 194–202.

6 Q. Liu, Z. F. Li, Y. Liu, H. Zhang, Y. Ren, C. J. Sun, W. Lu, Y. Zhou, L. Stanciu, E. A. Stach and J. Xie, *Nat. Commun.*, 2015, **6**, 6127–6137.

7 D. Kong, X. Li, Y. Zhang, X. Hai, B. Wang, X. Qiu, Q. Song, Q. H. Yang and L. Zhi, *Energy Environ. Sci.*, 2016, **9**, 906–911.

8 S. Kim, Z. Zhang, S. Wang, L. Yang, E. J. Cairns, J. E. Penner-Hahn and A. Deb, *J. Phys. Chem. C*, 2016, **120**, 7005–7012.

9 (*a*) Z. Liu, W. Peng, K. Shih, J. Wang, Z. Wang, H. Guo, G. Yan, X. Li and L. Song, *J. Power Sources*, 2016, **315**, 294–301; (*b*) J. Wang, X. Li, Z. Wang, B. Huang, Z. Wang and H. Guo, *J. Power Sources*, 2014, **251**, 325–330.

10 Z. K. Wang, J. Shu, Q. C. Zhu, B. Y. Cao, H. Chen, X. Y. Wu, B. M. Bartlett, K. X. Wang and J. S. Chen, *J. Power Sources*, 2016, **307**, 426–434.

11 H. T. Tan, X. Rui, W. Sun, Q. Yan and T. M. Lim, *Nanoscale*, 2015, **7**, 14595–14607.

12 L. Q. Mai, X. Xu, L. Xu, C. H. Han and Y. Z. Luo, *J. Mater. Res.*, 2011, **26**, 2175–2185.

13 X. Huang, X. Rui, H. H. Hng and Q. Yan, *Part. Part. Syst. Charact.*, 2015, **32**, 276–294.

14 D. J. Yan, X. D. Zhu, K. X. Wang, X. T. Gao, Y. J. Feng, K. N. Sun and Y. T. Liu, *J. Mater. Chem. A*, 2016, **4**, 4900–4907.

15 N. Steunou and J. Livage, *CrystEngComm*, 2015, **17**, 6780–6795.

16 (*a*) M. Srikanth, M. M. Rahman, L. H. Li, Q. Cai and Y. Chen, *RSC Adv.*, 2016, **6**, 35287–35294; (*b*) H. Song, C. Liu, C. Zhang and G. Cao, *Nano Energy*, 2016, **22**, 1–10; (*c*) H. Xu, J. Chen, H. Zhang, Y. Zhang, W. Li and Y. Wang, *J. Mater. Chem. A*, 2016, **4**, 4098–4106.

17 A. Pan, J. G. Zhang, Z. Nie, G. Cao, B. W. Arey, G. Li, S. Q. Liang and J. Liu, *J. Mater. Chem.*, 2010, **20**, 9193–9199.

18 L. Mai, L. Xu, C. Han, X. Xu, Y. Luo, S. Zhao and Y. Zhao, *Nano Lett.*, 2010, **10**, 4750–4755.

19 S. Liang, Y. Hu, Z. Nie, H. Huang, T. Chen, A. Pan and G. Cao, *Nano Energy*, 2015, **13**, 58–66.

20 (*a*) A. Pan, H. B. Hu, L. Yu, T. Zhu and X. W. Lou, *ACS Appl. Mater. Interfaces*, 2012, **4**, 3874–3879; (*b*) E. Uchaker, N. Zhou, Y. Li and G. Cao, *J. Phys. Chem. C*, 2013, **117**, 1621–1626.

21 C. Zhang, Z. Chen, Z. Guo and X. W. Lou, *Energy Environ. Sci.*, 2013, **6**, 974–978.

22 (*a*) Z. S. Ma, Z. C. Xie, Y. Wang, P. P. Zhang, Y. Pan, Y. C. Zhou and C. Lu, *J. Power Sources*, 2015, **290**, 114–122; (*b*) Z. Ma, X. Gao, Y. Wang and C. Lu, *J. Appl. Phys.*, 2016, **120**, 025302; (*c*) C. Wang, Z. Ma, Y. Wang and C. Lu, *J. Electrochem. Soc.*, 2016, **163**, A1157–A1163.

23 J. Liu, Y. Zhou, J. Wang, Y. Pan and D. Xue, *Chem. Commun.*, 2011, **47**, 10380–10382.

24 (*a*) X. W. Lou, L. A. Archer and Z. Yang, *Adv. Mater.*, 2008, **20**, 3987–4019; (*b*) A. Q. Pan, H. B. Wu, L. Zhang and X. W. Lou, *Energy Environ. Sci.*, 2013, **6**, 1476–1479.

25 A. M. Cao, J. S. Hu, H. P. Liang and L. J. Wan, *Angew. Chem., Int. Ed.*, 2005, **44**, 4391–4395.

26 Y. T. Wang, W. T. Whang and C. H. Chen, *ACS Appl. Mater. Interfaces*, 2015, **7**, 8480–8487.
27 (*a*) H. B. Wu, A. Pan, H. H. Hng and X. W. Lou, *Adv. Funct. Mater.*, 2013, **23**, 5669–5674; (*b*) L. Mai, Q. An, Q. Wei, J. Fei, P. Zhang, X. Xu, Y. Zhao, M. Yan, W. Wen and L. Xu, *Small*, 2014, **10**, 3032–3037.
28 A. Pan, H. B. Wu, L. Yu and X. W. Lou, *Angew. Chem., Int. Ed.*, 2013, **52**, 2226–2230.
29 A. Pan, T. Zhu, H. B. Wu and X. W. Lou, *Chem.–Eur. J.*, 2013, **19**, 494–500.
30 (*a*) S. Ge, B. Wang, J. Lin and L. Zhang, *CrystEngComm*, 2013, **15**, 721–728; (*b*) S. Cong, T. Sugahara, T. Wei, J. Jiu, Y. Hirose, S. Nagao and K. Suganuma, *Cryst. Growth Des.*, 2015, **15**, 4536–4542.
31 (*a*) N. V. Landschoot, E. M. Kelder and J. Schoonman, *J. Solid State Electrochem.*, 2003, **8**, 28–33; (*b*) S. Liang, Y. Yu, T. Chen, A. Pan, S. Zhang, J. Zhou, Y. Tang and X. Tan, *Mater. Lett.*, 2013, **109**, 92–95.
32 H. Pang, P. Cheng, H. Yang, J. Lu, C. X. Guo, G. Ning and C. M. Li, *Chem. Commun.*, 2013, **49**, 1536–1538.
33 (*a*) X. M. Cai, A. B. Djurisic, M. H. Xie, C. S. Chiu and S. Gwo, *Appl. Phys. Lett.*, 2005, **87**, 183103; (*b*) C. R. Bealing, W. J. Baumgardner, J. J. Choi, T. Hanrath and R. G. Hennig, *ACS Nano*, 2012, **6**, 2118–2127.
34 Q. An, P. Zhang, Q. Wei, L. He, F. Xiong, J. Sheng, Q. Wang and L. Mai, *J. Mater. Chem. A*, 2014, **2**, 3297–3302.
35 (*a*) Q. An, P. Zhang, F. Xiong, Q. Wei, J. Sheng, Q. Wang and L. Mai, *Nano Res.*, 2015, **8**, 481–490; (*b*) H. Song, C. Zhang, Y. Liu, C. Liu, X. Nan and G. Cao, *J. Power Sources*, 2015, **294**, 1–7.
36 (*a*) Y. Lu, J. Wu, J. Liu, M. Lei, S. Tang, P. Lu, L. Yang, H. Yang and Q. Yang, *ACS Appl. Mater. Interfaces*, 2015, **7**, 17433–17440; (*b*) G. Z. Fang, J. Zhou, Y. Hu, X. X. Cao, Y. Tang and S. Q. Liang, *J. Power Sources*, 2015, **275**, 694–701.